Supporting Information

Chen et al. 10.1073/pnas.1411154111

SI Methods

Two $^{57}Fe_7C_3$ samples were synthesized from 94% ^{57}Fe-enriched iron powder and graphite powder at 12 GPa and 1200 °C for 12–24 h using the multianvil apparatuses at the University of Michigan and GeoSoilEnviroCARS of the Advanced Photon Source (APS), Argonne National Laboratory (ANL). Grains were hand picked from the run products and screened by X-ray diffraction (XRD) for structural confirmation and detection of impurities such as excess Fe or other carbides. Pure Fe_7C_3 grains with the expected $P6_3mc$ structure and cell parameters (1) were then selected for the experiments.

Three panoramic diamond anvil cells (DAC) with 100/300 μm (Run 2A), 150/300 μm (Run 2B), and 250/370 μm (Run 3A) beveled diamonds were used to generate high pressures for nuclear resonant inelastic X-ray scattering (NRIXS), synchrotron Mössbauer spectroscopy (SMS), and XRD measurements (Table S1). We placed a tungsten carbide backing plate on the upstream side of the X-rays and a cubic boron nitride backing plate on the downstream side, to observe XRD of the sample at 14.4125 keV (2). Polycrystalline $^{57}Fe_7C_3$ samples were loaded inside a boron nitride epoxy insert, which filled a hole in a preindented beryllium gasket. The sample thickness is ∼30 μm thick in Run 2A, ∼25 μm in Run 2B, and ∼10 μm in Run 3A. The boron nitride epoxy insert helps reduce axial pressure gradient and maintain sample thickness so that sufficient count rate can be achieved at high pressures (3). Each sample is sandwiched between two thin NaCl layers, which help further reduce the deviatoric stress and prevent bridging between the sample and diamond anvil. A few ruby spheres were placed next to the sample and served as pressure markers below 110 GPa (4) (Table S1). In Run 2A, on the cylinder side of the diamond anvil cell, a small amount of gold powder was placed near the sample, serving as a secondary pressure marker above 70 GPa (5). The Raman spectra of the diamond anvils were collected as a complementary pressure gauge before and after each measurement at pressures higher than 70 GPa (6). The discrepancies between gold and diamond pressures are within ±5 GPa, even at the highest pressure achieved in this study.

The NRIXS and SMS measurements were carried out at Sector 3 of APS, with the storage ring operating in the top-up mode with 24 bunches that were separated by 153 ns (7). A high-resolution monochromator was tuned around the nuclear resonance energy of ^{57}Fe at 14.4125 keV with a step size of 0.25 meV and a collection time of 3–5 s per energy step. The SMS measurements were conducted before or after each NRIXS measurement using the APD detector placed downstream in the forward scattering direction. XRD data were collected before and after each NRIXS measurement to determine the pressure.

The partial phonon density of states (PDOS) of Fe_7C_3 up to 154 GPa were derived from the NRIXS data using the PHOENIX program package (8) (Fig. S1). For harmonic solids, a parabolic fitting of the low-energy portion of PDOS provides an approximation to the bulk Debye sound velocity (v_D), even though the obtained PDOS for iron only gives part of the lattice dynamics of the material (9). After applying a correction factor for the density difference due to the ^{57}Fe enrichment of the sample, the v_D was then determined using the psvl program in the PHOENIX program. The optimal energy range of each spectrum has its low end between 3 meV and 5 meV and the high end between 10 meV and 16 meV (Fig. S1 and Table S1) (10), which was selected to minimize the χ^2 value of the parabolic fitting and achieve an uncertainty of less than 2% in v_D. The equation of state of Fe_7C_3 (11) was used to calculate the unit cell volumes and served as the input parameters to the psvl program at a given pressure. Using the v_D from the NRIXS measurements and the existing density (ρ) and isothermal bulk modulus (K_T) data (11), we derived the v_P and v_S of isotropic aggregate of Fe_7C_3 using the following relations (10):

$$\frac{3}{v_D^3} = \frac{1}{v_P^3} + \frac{2}{v_S^3} \quad \text{[S1]}$$

$$\frac{K_S}{\rho} = v_P^2 - \frac{4}{3}v_S^2 \quad \text{[S2]}$$

$$\frac{G}{\rho} = v_S^2, \quad \text{[S3]}$$

where the adiabatic bulk modulus (K_S) is approximated by K_T (K_T and K_S differ by less than 1%) (Fig. 3).

The X-ray emission spectroscopy (XES) measurements of Fe_7C_3 were conducted in Sector 16-ID-D of APS. The samples were immersed in neon or boron nitride epoxy and compressed in symmetric DACs. Ruby spheres were placed in the vicinity of the sample and served as the pressure marker. The measurements adopted a Rowland circle configuration with a spherical silicon (4 4 0) crystal and used a helium tube to reduce scattering by air (12). XES spectra were normalized to unity in integrated intensity and aligned at the K_β peak in energy (Fig. S2). The intensity of the satellite peak (K'_β) began to decrease between 10 GPa and 17 GPa, reached the lowest value by 53 GPa, and remained the same upon further compression, indicating a gradual transition from high spin (HS) to low spin (LS) between 10 GPa and 53 GPa. Using the spectrum at the highest pressure of 94(±5) GPa as the reference for the LS state, we calculated the integrated spectral area from 7035 eV to 7055 eV of each spectrum and used the difference between the calculated area and that of the reference LS state as a proxy for the total spin momentum (12–15) (Fig. 2*B*).

SI Thermodynamic and Vibrational Properties

From the phonon DOS results, we extracted elastic, thermodynamic and vibrational parameters of the Fe component in Fe_7C_3, including the mean force constant (D_{av}), Lamb–Mössbauer factor (f_{LM}), vibrational specific heat (C_{vib}), vibrational entropy (S_{vib}), critical temperature (T_c), and kinetic energy E_k at 300 K and E_z at 0 K (Fig. S4). Pronounced changes occurred in all parameters near 53 GPa where the gradual spin-pairing transition completes. We observed dips in T_c, D_{av}, f_{LM}, E_k, and E_z, similar to those in the sound velocities and shear modulus, indicating their common origin from changes in atomic radius and bonding nature across the transition.

SI Effect of Nonhydrostaticity on the Sound Velocities

Nonhydrostaticity due to the use of a solid pressure-transmitting medium may give rise to elevated deviatoric stresses under high pressures, thus introducing uncertainties in measured physical properties. While almost all NRIXS measurements above 1 Mbar were conducted under nonhydrostatic conditions, efforts have been made to mitigate the effects from nonhydrostaticity by using He or Ne as the pressure-transmitting medium to generate quasihydrostatic conditions (16–18). The v_D of iron under quasihydrostatic conditions up to 136 GPa (18) are systematically

higher than the datasets collected under nonhydrostatic conditions, by ~3% (16) and 8% (19), respectively. In our measurements, efforts have been made to reduce the deviatoric stress by using boron nitride epoxy insert and sandwiching the samples between two NaCl layers. If the reported nonhydrostatic effects are applicable to our datasets, the reduction of v_D of Fe_7C_3 due to nonhydrostaticity is approximately at the level of ~3% and probably less than ~8%. Although the measured v_D of compressed Fe_7C_3 may be slightly lower than that at hydrostatic or quasi-hydrostatic conditions, the observed shear softening leads to a reduction in v_S by more than 25%, well beyond the effect of nonhydrostaticity. Owing to potentially higher values of v_S for both iron and Fe_7C_3 under hydrostatic conditions, slightly larger volume fraction of Fe_7C_3 than estimated from nonhydrostatic datasets would be required to reduce v_S of the inner core to PREM values, further supporting the Fe_7C_3 inner core model.

1. Herbstein F, Snyman J (1964) Identification of Eckstrom–Adcock iron carbide as Fe_7C_3. *Inorg Chem* 3:894–896.
2. Gao L, et al. (2011) Effect of temperature on sound velocities of compressed Fe_3C, a candidate component of the Earth's inner core. *Earth Planet Sci Lett* 309:213–220.
3. Lin J-F, Shu J, Mao HK, Hemley RJ, Shen G (2003) Amorphous boron gasket in diamond anvil cell research. *Rev Sci Instrum* 74:4732.
4. Mao HK, Xu J, Bell PM (1986) Calibration of the ruby pressure gauge to 800 kbar under quasi-hydrostatic conditions. *J Geophys Res* 91:4673–4676.
5. Takemura K, Dewaele A (2008) Isothermal equation of state for gold with a He-pressure medium. *Phys Rev B* 78:104119.
6. Akahama Y, Kawamura H (2004) High-pressure Raman spectroscopy of diamond anvils to 250 GPa: Method for pressure determination in the multimegabar pressure range. *J Appl Phys* 96:3748–3751.
7. Sturhahn W (2004) Nuclear resonant spectroscopy. *J Phys Condens Matter* 16:497–530.
8. Sturhahn W (2000) CONUSS and PHOENIX: Evaluation of nuclear resonant scattering data. *Hyperfine Interact* 125:149–172.
9. Hu MY, et al. (2003) Measuring velocity of sound with nuclear resonant inelastic X-ray scattering. *Phys Rev B* 67:094304.
10. Sturhahn W, Jackson JM (2007) Geophysical applications of nuclear resonant spectroscopy. *Geological Society of America Special Papers* 421:157–174.
11. Chen B, et al. (2012) Magneto-elastic coupling in compressed Fe_7C_3 supports carbon in Earth's inner core. *Geophys Res Lett* 39:L18301.
12. Rueff JP, et al. (1999) Pressure-induced high-spin to low-spin transition in FeS evidenced by X-ray emission spectroscopy. *Phys Rev Lett* 82:3284–3287.
13. Lin J-F, et al. (2004) Magnetic transition in compressed Fe_3C from X-ray emission spectroscopy. *Phys Rev B* 70(21):212405.
14. Lin J-F, et al. (2007) Spin transition zone in Earth's lower mantle. *Science* 317(5845): 1740–1743.
15. Li J, et al. (2004) Electronic spin state of iron in lower mantle perovskite. *Proc Natl Acad Sci USA* 101(39):14027–14030.
16. Murphy CA, Jackson JM, Sturhahn W, Chen B (2011) Grüneisen parameter of hcp-Fe to 171 GPa. *Geophys Res Lett* 38:L24306.
17. Murphy CA, Jackson JM, Sturhahn W, Chen B (2011) Melting and thermal pressure of hcp-Fe from the phonon density of states. *Phys Earth Planet Inter* 188:114–120.
18. Gleason AE, Mao WL, Zhao JY (2013) Sound velocities for hexagonally close-packed iron compressed hydrostatically to 136 GPa from phonon density of states. *Geophys Res Lett* 40:2983–2987.
19. Mao HK, et al. (2001) Phonon density of states of iron up to 153 gigapascals. *Science* 292(5518):914–916.

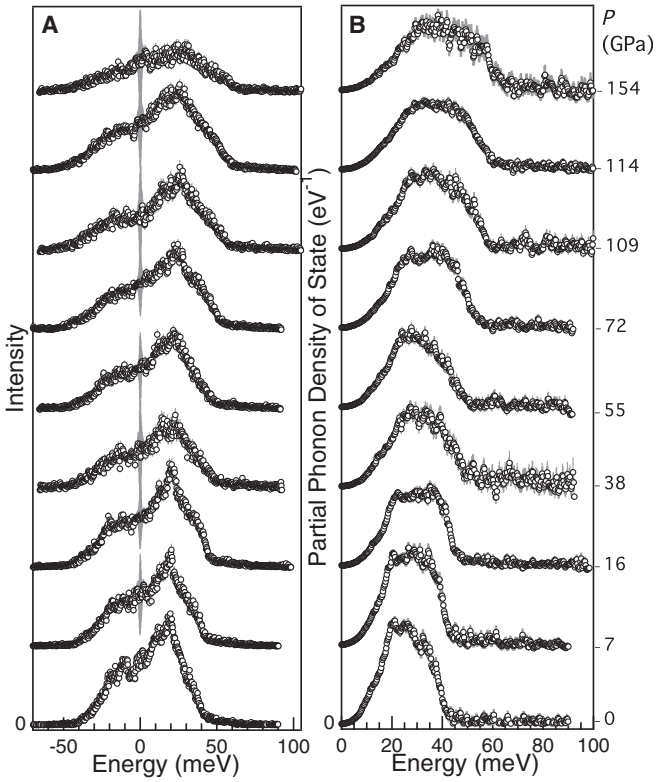

Fig. S1. Nuclear Resonant Inelastic X-ray Scattering (NRIXS) spectra and partial phonon density of state (DOS) of Fe_7C_3 up to 154 GPa and at 300 K. (*A*) NRIXS data, with the elastic peak at zero energy (corresponding to ^{57}Fe nuclear resonant energy) removed. (*B*) Derived partial phonon DOS. The low-energy region of the DOS, with optimal energy range from 3–5 to meV 10–16 meV, is used to derive v_D. The spectra at high pressures are vertically shifted for clarity.

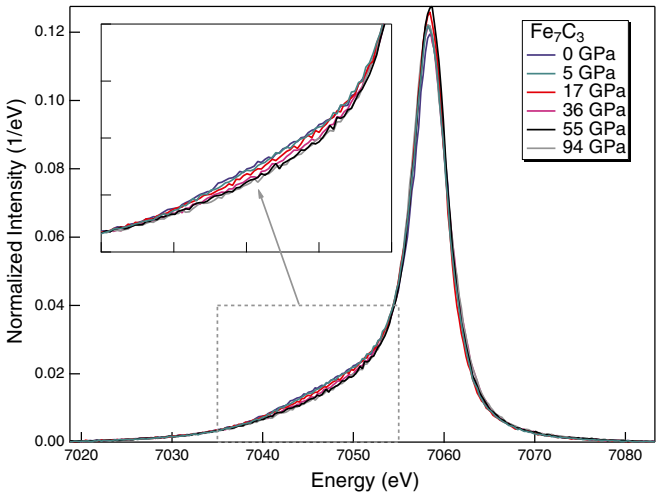

Fig. S2. Selected Fe-K_β fluorescence spectra of Fe_7C_3 up to 94 GPa and at 300 K. The XES spectra were normalized to unity in integrated intensity. The inset shows the satellite emission peak (K'_β) between 7,035 and 7,055 eV. Similar to Fe_3C (13), the intensity of K'_β peak in Fe_7C_3 in the lower-energy region of the main emission peak (K_β) is not as intense as that in Mott insulators. The changes of the satellite peak intensity in Fe_7C_3 (this study) and other iron-rich alloys attributed to the high-spin to low-spin transition (e.g., refs. 12 and 13) are much more subtle compared with oxides and silicates (14, 15). Nevertheless, the disappearance of the satellite peak has been used as a robust criterion for the high-spin to low-spin magnetic transition in metals and alloys (13).

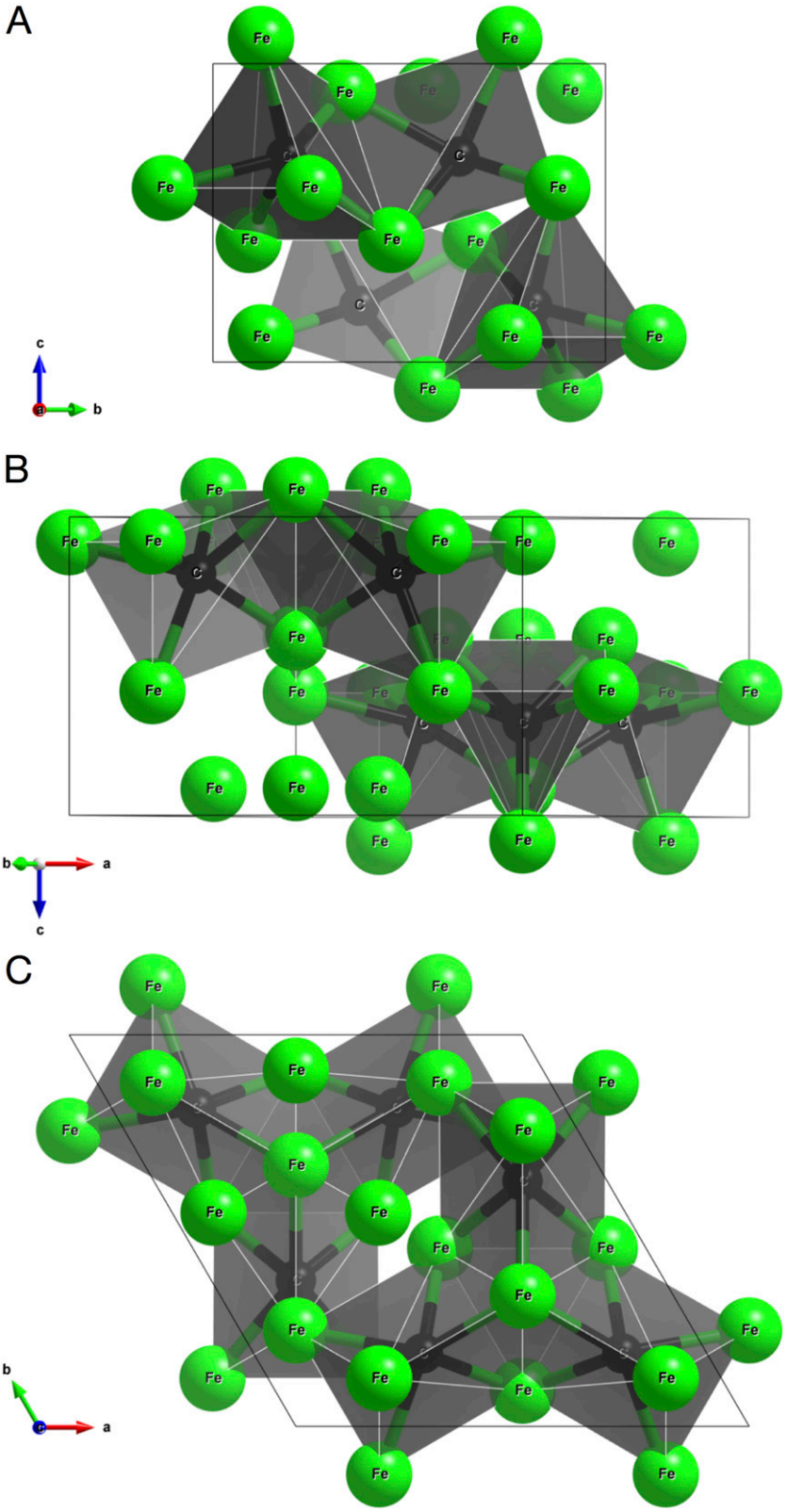

Fig. S3. Crystal structure of Fe_7C_3 with hexagonal symmetry (space group: $P6_3mc$) projected (*A*) along a axis, (*B*) perpendicular to the (10 $\bar{1}$0) plane, and (*C*) along *c* axis. The coordinates of iron and carbon atoms are from Fang et al. (1). Iron has three distinct sites (green): Wykcoff sites 2b, 6c, and 6c; carbon only has one site (black): Wykcoff sites 6c. The carbon atom is located at the center of the ditrigonal prism formed by six iron atoms.

1. Fang CM, van Huis MA, Zandbergen HW (2009) Structural, electronic, and magnetic properties of iron carbide Fe_7C_3 phases from first-principles theory. *Phys Rev B* 80:224108.

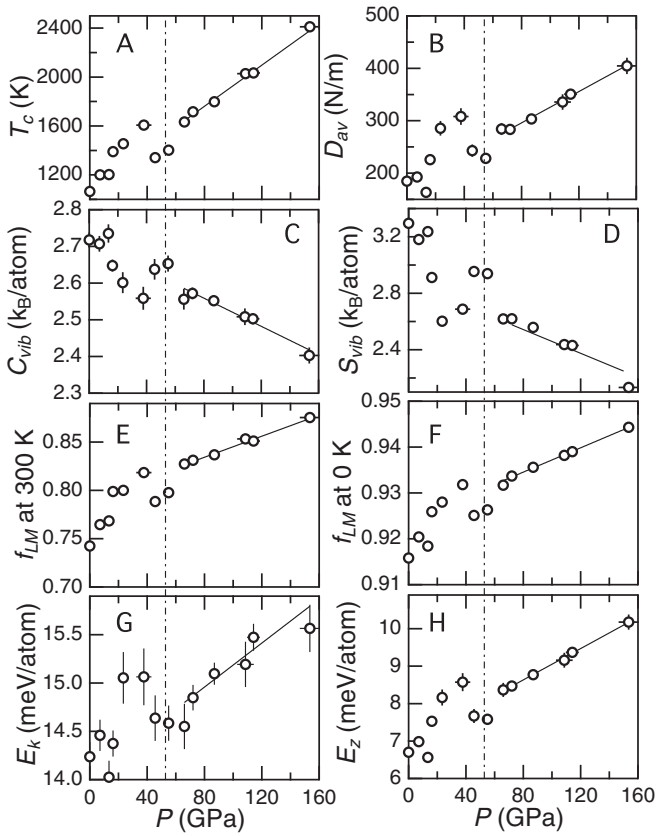

Fig. S4. Elastic, vibrational, and thermodynamic parameters of Fe_7C_3 up to 154 GPa and at 300 K. (*A*) Mean force constant, D_{av} (N/m). (*B*) Critical temperature, T_c (K). (*C*) Vibrational specific heat, C_{vib} (k_B/atom; k_B is Boltzmann constant). (*D*) Vibrational entropy, S_{vib} (k_B/atom). (*E*) Lamb–Mössbauer factor at 0 K and (*F*) Lamb–Mössbauer factor at 300 K, f_{LM}. (*G*) Kinetic energy at 300 K, E_k (meV/atom). (*H*) Kinetic energy at 0 K, E_z (meV/atom). The dot-dashed lines depict that a graduate spin-pairing transition completes near 53 GPa (11).

Table S1. Sound velocity, density, and shear modulus of Fe_7C_3 up to 154 GPa and at 300 K

Run No.	P,* GPa	Energy Range,† meV	v_D, km·s^{-1}	v_P, km·s^{-1}	v_S, km·s^{-1}	G, GPa	ρ,‡ g·cm^{-3}
2A-P0	0.0(0.0)	2.7–9.7	3.061(0.030)	6.017(0.027)	2.714(0.028)	56.1(1.2)	7.617(0.004)
2A-P1	7.1(0.2)	3.2–13.2	3.163(0.033)	6.287(0.032)	2.803(0.030)	61.8(1.3)	7.870(0.005)
3A-P1	13.4(0.1)	2.8–10.3	3.282(0.056)	6.947(0.255)	2.902(0.051)	68.2(2.4)	8.102(0.026)
2A-P2	16.2(0.5)	3.8–12.5	3.414(0.033)	7.149(0.273)	3.020(0.031)	74.5(1.5)	8.172(0.030)
3A-P2	23.4(1.7)	2.7–11.5	3.438(0.051)	7.507(0.325)	3.036(0.046)	77.0(2.3)	8.350(0.043)
3A-P3	37.7(5.3)	3.2–12.0	3.500(0.042)	8.110(0.404)	3.085(0.038)	82.3(2.0)	8.645(0.065)
2B-P2	45.6(3.1)	2.7–11.5	3.244(0.042)	8.280(0.447)	2.853(0.038)	71.5(1.9)	8.788(0.077)
2B-P1	55.0(2.5)	2.7–11.5	3.301(0.022)	7.979(0.103)	2.906(0.020)	75.6(1.0)	8.947(0.024)
2B-P3	66.0(2.3)	2.5–11.2	3.484(0.027)	8.188(0.110)	3.070(0.025)	86.2(1.4)	9.152(0.028)
2A-P3	72.0§(2.0)	2.7–15.2	3.491(0.016)	8.257(0.115)	3.076(0.015)	87.6(0.8)	9.262(0.033)
2A-P4	86.9§(3.5)	4.8–13.5	3.586(0.063)	8.452(0.128)	3.159(0.057)	95.1(3.4)	9.526(0.038)
2B-P4	108.6(5.8)	5.4–16.2	3.726(0.074)	8.711(0.143)	3.284(0.066)	106.6(4.3)	9.887(0.044)
2A-P5	114.2§(4.5)	5.2–14.0	3.697(0.065)	8.743(0.147)	3.257(0.059)	105.8(3.8)	9.974(0.049)
2A-P6	153.5§(7.0)	3.8–16.3	3.860(0.019)	9.108(0.171)	3.401(0.018)	122.4(1.3)	10.582(0.064)

*Pressures were determined from fluorescence spectra of small ruby spheres placed close to the sample in NaCl pressure medium (4).
†The optimal energy range of each spectrum that was selected to minimize the χ^2 value of the parabolic fitting and to achieve an uncertainty of less than 2% in v_D.
‡Densities were calculated according to the equation of state of Fe_7C_3 (11).
§Pressures were determined from the equation of state of gold placed near the sample (5).